



## Calhoun: The NPS Institutional Archive

---

Faculty and Researcher Publications

Funded by Naval Postgraduate School

---

2016

# Photonic-Assisted Error-Free Wireless Communication With Multipath Precompensation Covering 2–18 GHz

Li, Yihan

---

<http://hdl.handle.net/10945/52408>



Calhoun is a project of the Dudley Knox Library at NPS, furthering the precepts and goals of open government and government transparency. All information contained herein has been approved for release by the NPS Public Affairs Officer.

**Dudley Knox Library / Naval Postgraduate School**  
**411 Dyer Road / 1 University Circle**  
**Monterey, California USA 93943**

<http://www.nps.edu/library>

# Photonic-Assisted Error-Free Wireless Communication With Multipath Precompensation Covering 2–18 GHz

Yihan Li, *Member, OSA* and Andrew M. Weiner, *Fellow, OSA*

**Abstract**—A wireless communication experiment that uses photonic-assisted radio-frequency arbitrary waveform generation (RF-AWG) for precompensation of multipath distortion over a 2–18 GHz frequency band is reported. Photonic-assisted RF-AWG is used both for spread spectrum sounding of the multipath channel and for synthesis of precompensation waveforms that yield pulse compression and distortion suppression at the receiver. By directly encoding the precompensated waveforms in optical hardware, 250 Mbit/s error-free data transmission is achieved experimentally in binary-phase-shift-keying format. For the first time to our knowledge, phase compensation and time reversal precompensation techniques are compared in hardware encoded data transmission experiments; our results confirm predictions that phase compensation outperforms time reversal under intersymbol interference limited conditions.

**Index Terms**—Microwave communications, multipath channel, optical pulse shaping.

## I. INTRODUCTION

ULTRA-WIDEBAND (UWB) has drawn substantial research attention from both academia and industry [1]–[4]. Its enormous available bandwidth offers ultrashort temporal resolution, empowering applications such as ultra-fine resolution positioning [5] and high speed wireless communication [3], [6]. UWB is characterized by a noise-like signal spectrum, jamming resistance, and potentially low complexity and cost [4]. From a communication point of view, there have been extensive studies in signal synthesis and wireless data transmission in the 3.1–10.6 GHz frequency range. Refs. [7]–[10] have demonstrated the use of photonics for data generation and wired optical fiber distribution of UWB signals, together with free space transmission over simple wireless channels. However, in practical wireless scenarios, multipath signal distortion may severely degrade the performance of UWB communication systems through intersymbol interference (ISI). Consequently, multipath compen-

sation is required. On-line precompensation at the transmitter is often preferred as it enables a simpler receiver structure. Naqvi *et al.* [11] conducted experiments in which time reversal (TR) is implemented in order to precompensate for multipath distortion over a 2 GHz bandwidth from 0.7 to 2.7 GHz, just below the UWB band. Although precompensation is effective at low data rates, at higher data rates an error floor was observed, e.g., bit error rates (BER)  $>10^{-2}$  for 250 Mb/s data rate, and was attributed to ISI. In this paper we report the use of photonic-assisted radio frequency arbitrary waveform generation to perform multipath compensation and wireless communication with signals stretching from 2 to 18 GHz, easily covering the full UWB band. By employing a phase compensation (PC) algorithm, we achieve error-free wireless transmission at 250 Mb/s data rate over a strong multipath channel (the bit error rate is bounded at  $8 \times 10^{-6}$  or below by the PN-sequence length equal to  $2^{17} - 1$ ). Our work, the first to compare the performance of TR and PC directly in data transmission experiments, confirms the prediction [12] that PC provides substantial superiority over TR in terms of ISI suppression. A preliminary description of our work covering PC only was reported in [13]. Here we provide improved and substantially broader results, discussing both PC and TR studies and reporting and contrasting bit error rate curves and distribution functions of the received signals.

To realize on-line precompensation, an arbitrary waveform generator (AWG) is essential, for the reason that the impulse response of a multipath UWB channel is often highly complex (wide RF bandwidth and long temporal duration) and may change drastically with even a few centimeters of antenna spatial displacement [14]. Electrical AWG offers long record length but restricted RF bandwidth due to speed limitations in digital-to-analogue conversion. In contrast, radio-frequency arbitrary waveform generation (RF-AWG) based on photonic techniques, especially those utilizing optical pulse shaping [15] and frequency-to-time mapping [16], [17], have experimentally demonstrated tens of GHz of RF bandwidth at center frequencies up to  $\sim 100$  GHz [18], [19]. In addition, its inherent compatibility with radio-over-fiber technology considerably reduces signal power loss during wired distribution [9].

In this work, we use photonics-based RF-AWG both for channel sounding and for wireless communications experiments implementing multipath precompensation. Our system first generates a spread spectrum sounding waveform to characterize the impulse response of the wireless channel with rich multipath. The channel information is then utilized by our photonic RF-AWG to synthesize pre-distorted input waveforms which

Manuscript received April 10, 2016; revised July 07, 2016; accepted July 12, 2016. Date of publication July 12, 2016; date of current version August 12, 2016. This work was supported in part by the Office of the Assistant Secretary of Defense for Research and Engineering under the National Security Science and Engineering Faculty Fellowship program from the Naval Postgraduate School under Grant N00244-09-1-0068.

Y. Li was with the Ultrafast Optical and Optical Communications Laboratory, Purdue University, West Lafayette, IN 47907 USA. He is now with IMRA America, Inc., Longmont, CO 80501 USA (e-mail: yli@imra.com).

A. M. Weiner is with the Ultrafast Optical and Optical Communications Laboratory, Purdue University, West Lafayette, IN 47907 USA (e-mail: amw@purdue.edu).

Color versions of one or more of the figures in this paper are available online at <http://ieeexplore.ieee.org>.

Digital Object Identifier 10.1109/JLT.2016.2591438

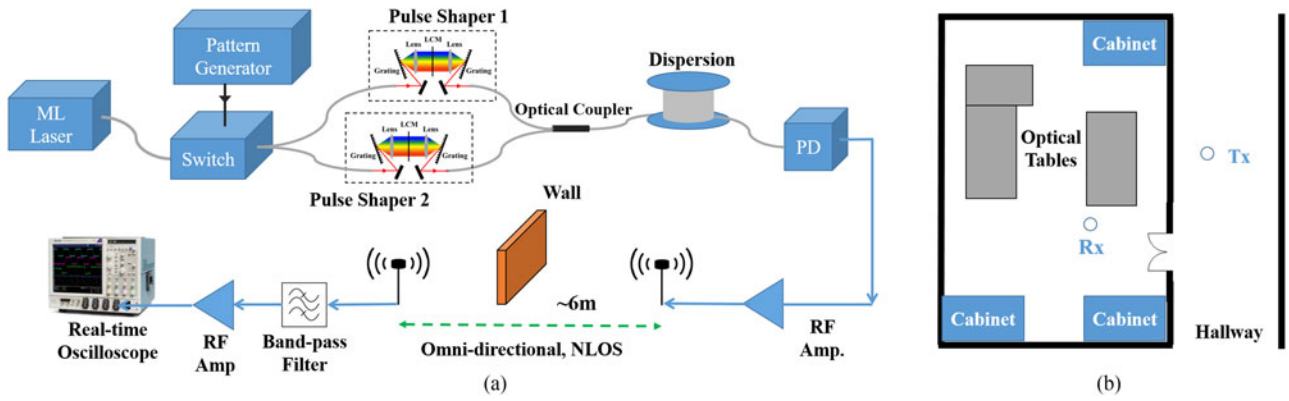


Fig. 1. (a) Block diagram of the experimental apparatus. ML: mode-locked; PD: photodetector; Amp: amplifier. (b) Environmental layout of the transmitter and receiver.

self-compress while propagating through the communication channel and arrive at the receiver in the form of short pulses. Moreover, since the data stream is directly encoded onto the optical pulses before they are stretched and converted into RF compensation waveforms, our system is capable of both data modulation in real time and channel compensation with waveforms longer than the bit period, enabling high data rate communication and strong ISI suppression. In essence, our photonic subsystem performs an automatic hardware convolution between the applied data sequence and the precompensation waveform. This eliminates the need for the potentially time consuming off-line computation of this convolution that would be required in the case of precompensation experiments based on an electrical AWG.

## II. EXPERIMENTAL SETUP

The experimental setup is sketched in Fig. 1(a). Ultrashort optical pulses generated by a commercial mode-locked laser (Menlo Systems FC1500-250-WG) at 250 MHz repetition are used as our source. These pulses are switched into one of two commercial fiber-pigtailed pulse shapers (Finisar 1000S) by an optical switch block, which is controlled by a pattern generator that is synchronized to the laser repetition rate. In each pulse shaper the amplitude and phase applied to the optical spectrum can be arbitrarily set. The two pulse shapers are programmed in anti-phase to ensure that waveforms generated from the two arms have opposite polarity but are otherwise ideally identical after optical-to-electrical conversion later in the scheme. Subsequently, the optical signals in the two arms are combined by a fiberized polarization beam combiner for minimum optical interference. After propagating through a spool of single mode fiber whose length is chosen to provide the desired chromatic dispersion, the intensity of each optical pulse becomes a scaled replica of the spectrum stretched to the nanosecond time scale. In our experiment, both channel sounding and precompensation waveforms are implemented with an identical 7.5 ns time aperture. The stretched optical pulses are then converted into electrical signals by a photodetector (DSC 30S). This results in a user programmable electrical waveform that repeats at 250 MHz, onto which binary phase-shift keying (BPSK) data

modulation is imposed at 250 Mb/s. The generated electrical signal is amplified by an RF amplifier (Minicircuits ZVA-183) and transmitted into our wireless channel. The channel consists of two omni-directional antennas (EM 6865) separated by  $\sim 6$  m in a non-line-of-sight geometry. The detailed orientation of the transceiver is depicted in Fig. 1(b). The received RF signal is filtered by a band-pass filter (K&L, 2-18 GHz) and amplified by a low-noise amplifier (LNA, B&Z 120UD1) before being recorded by a real-time oscilloscope (Tektronix 72004B) with a sampling period of 20 ps.

## III. CHANNEL SOUNDING

To characterize the impulse response of the data communication system, including the wireless channel, filter and RF amplifiers, we first program the pulse shapers and select appropriate amount of dispersion to generate linear frequency-chirped sounding waveform covering 2–18 GHz with a time-aperture of 7.5 ns. To ensure that the repetition period of the sounding waveform safely exceeds the delay spread of the multipath channel, a length-127 pseudorandom (PN) sequence modulation is applied to the switch block to expand the repetition from 4 ns to  $> 500$  ns [20]. Such a modulated spread spectrum signal is utilized to excite the system, and both the input and output waveforms are captured by the real-time oscilloscope. For illustration purposes only, we first show the waveform after PN modulation with a shorter dispersive fiber, for which the time aperture of the chirp waveform equals the pulse repetition period. (This avoids showing the complicated and less intuitive pattern that results with our actual sounding waveform for which adjacent chirp waveforms overlap.) A 20 ns measurement segment, consisting of five frequency-chirped waveforms with the imposed phase modulation, is shown in Fig. 2(a). In the expanded view of the last 0.6 ns of each chirped waveform [shaded in gray in Fig. 2(a)], the polarities of the individual chirped waveforms can be observed to be “-1, 1, 1, -1, -1”. The spectrogram of Fig. 2(a), computed offline from the temporal measurement, is plotted in Fig. 2(b). We reiterate that in the actual experiments, the time aperture of the sounding waveform is chosen to be 7.5 ns, matching that of the precompensation waveform. The spectrogram of the actual sounding waveform is plotted in

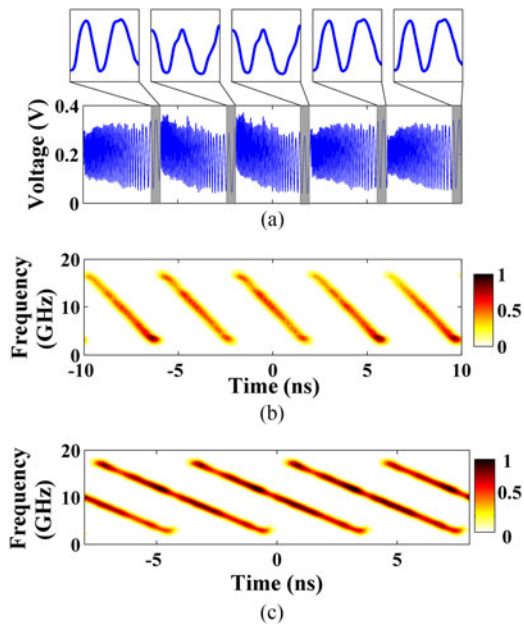


Fig. 2. Spread spectrum channel sounding signal. (a) Temporal measurement of the 4 ns chirped waveform consisting of five periods. Insets: magnifications of the last 0.6 ns [shaded in gray in Fig. 2(a)] of each chirped waveform. (b) Spectrogram of Fig. 2(a). (c) Spectrogram of the 7.5 ns sounding waveform consisting of four periods.

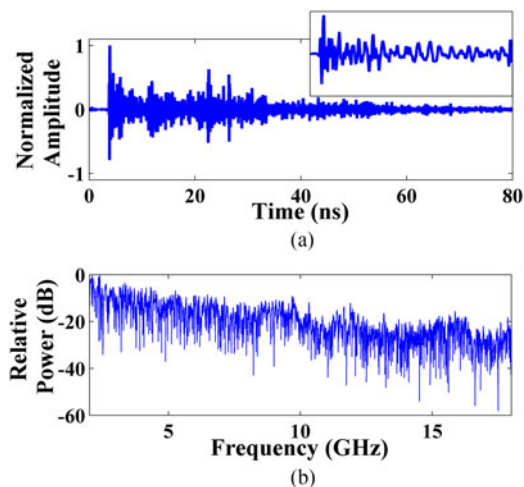


Fig. 3. Calculated wireless channel information based on transmitted and received spread spectrum waveforms. (a) Impulse response. RMS delay spread  $\sim 17.1$  ns. Inset: magnification of the first 8 ns of the impulse response. (b) Frequency response from 2 to 18 GHz.

Fig. 2(c). From this visualization we clearly observe that the time apertures of the individual chirp waveforms exceed their time separation; hence the overall waveform consists of time-delayed overlapped linear down chirp signals with PN-sequence polarity reversals.

We employ a deconvolution algorithm [21] to retrieve the impulse response as well as the frequency response of the system, as shown in Fig. 3(a) and (b), respectively. It can be clearly observed that, as the transmitted waveform arrives at the receiver via different paths, the impulse response is significantly stretched in time, with a RMS delay spread of  $\sim 17.1$  ns. The

frequency response demonstrates stronger attenuation at higher frequencies and numerous deep fades, which serve as another evidence of rich multipath.

As in our group's previous work [12], [22], in the current experiments the received sounding waveform at the receiver (Rx) is communicated back to the transmitter (Tx) through Ethernet cable or wireless LAN for channel impulse response analysis. In this case, both the sounding waveform and the data-encoded pre-compensation waveform (to be discussed in Section IV) are transmitted from Tx to Rx. Alternatively, by exploiting the reciprocity property of UWB [23], one might choose to perform the channel characterization in a reversed way - directly transmitting the sounding waveform from the original receiver (Rx) to the original transmitter (Tx) over the UWB channel, after which the original Tx performs the channel impulse response analysis and generates the pre-compensation waveform. In this case, the sounding waveform and the data-encoded pre-compensation waveform travel in opposite directions - from Rx to Tx for the former, and from Tx to Rx for the latter. The reciprocity property guarantees that the impulse response of the UWB channel can be retrieved and the self-compression should still be achieved.

#### IV. DATA TRANSMISSION WITH PRECOMPENSATION

In order to enable pulse compression at the receiver, we first compute the target input waveform by applying a PC algorithm offline to the measured impulse response. Through canceling the frequency-dependent phase variation of the transmission channel, the PC algorithm generates a pre-distorted waveform which self-compresses while propagating and arrives at the receiver with a strong peaking effect. Compared to TR, PC is more effective at sidelobe reduction and thus improves ISI suppression [12]. If we denote the impulse and frequency response of the system by  $h_{\text{sys}}(t)$  and  $H_{\text{sys}}(f)$ , respectively, the phase-compensated waveform can be expressed as

$$h_{\text{pc}}(t) = \mathcal{F}^{-1} \{ e^{-j\angle H_{\text{sys}}(f)} \}, \quad (1)$$

where  $\mathcal{F}^{-1}$  denotes inverse Fourier transform. Capitalizing on the arbitrary programmability of our photonic RF-AWG, we then program the pulse shapers and choose the amount of dispersion accordingly to synthesize a truncated version of the pre-distortion waveform. In the current experiments we truncate the pre-distorted waveform to a time aperture of 7.5 ns, which is already sufficient to realize high quality compression at the receiver. The compensation waveform is selected to have the same temporal duration as the sounding waveform, allowing channel sounding and data transmission to use the same dispersive fiber. This generated waveform is modulated and transmitted into the communication system. The input signal can be mathematically expressed as

$$h_{\text{in-pc}}(t) = \sum_i d_i \cdot \delta(t - iT) * h_{\text{pc}}(t), \quad (2)$$

where  $d_i$  is the  $i$ -th element of the data sequence,  $d_i \in \{1, -1\}$ , and  $T$  denotes the bit period. In our experiment, we use a pseudo-random sequence of length  $2^{17} - 1$  as the data sequence (limited by the record length of our real-time oscilloscope). As mentioned earlier, one advantage of our photonic approach is that

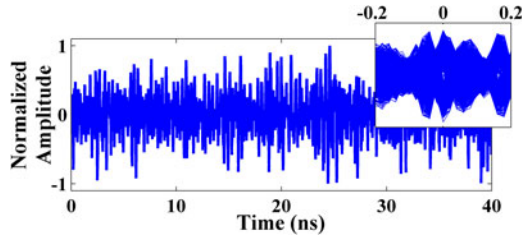


Fig. 4. Ten bit periods of the simulated received waveform with short pulses as input. Inset: eye diagram consisting of 1023 overlapped traces, 0.4 ns horizontal span.

the convolution indicated in Eq. (2) occurs automatically in the photonic hardware, without the need for potentially time consuming off-line computation. The output signal resulting from phase precompensation can be expressed as

$$\begin{aligned} h_{\text{out\_pc}}(t) &= h_{\text{in\_pc}}(t) * h_{\text{sys}}(t) \\ &= \sum_i d_i \cdot \delta(t - iT) * h_{\text{pc}}(t) * h_{\text{sys}}(t) \\ &= \sum_i d_i \cdot \delta(t - iT) * \mathcal{F}^{-1} \{|H_{\text{sys}}(f)|\}. \end{aligned} \quad (3)$$

Equation (3) clearly reveals the abovementioned cancellation of frequency-dependent phase variation of the transmission system.

In the case of TR [6], [24], the pre-distorted compensation waveform is just the temporal reversed version of the impulse response. Mathematically, it can be expressed as

$$h_{\text{tr}}(t) = h_{\text{sys}}(-t) = \mathcal{F}^{-1} \{H_{\text{sys}}^*(f)\}. \quad (4)$$

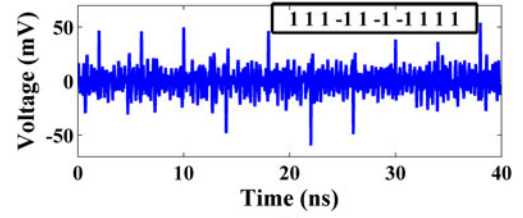
Following the previous derivation procedure, the output signal when TR is applied becomes

$$\begin{aligned} h_{\text{out\_tr}}(t) &= h_{\text{in\_tr}}(t) * h_{\text{sys}}(t) \\ &= \sum_i d_i \cdot \delta(t - iT) * \mathcal{F}^{-1} \{|H_{\text{sys}}(f)|^2\}. \end{aligned} \quad (5)$$

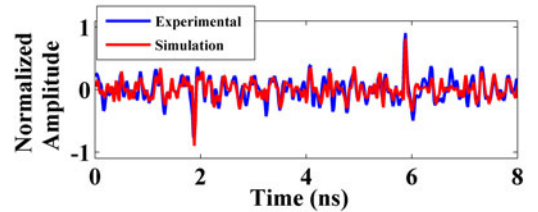
Again the frequency-dependent phase variation is removed. However, the output signal now contains a squared spectral magnitude. As pointed out in [12], this squaring operation increases the spectral intensity variation evident for example in Fig. 3(b), leading to higher sidelobe levels in pulse compression and aggravating ISI.

## V. EXPERIMENTAL RESULTS OF PHASE COMPENSATION

Here we evaluate the received waveforms with and without precompensation. Experimental comparison has been made for on-off-keying over a similar channel in [13], and significant improvement is observed when precompensation is utilized. In this paper we consider BPSK modulation. We first simulate the ideal (noise-free) situation without precompensation by convolving a train of 1023 encoded short pulses repeated every 4 ns with the retrieved impulse response shown in Fig. 3(a). A 40 ns long result is plotted in Fig. 4; the inset is the eye diagram synthesized by overlapping multiple bit periods in the same temporal frame. The obvious severe signal degradation makes it practically im-



(a)



(b)

Fig. 5. (a) Ten bit periods of the received signal with BPSK data modulation, 7.5 ns phase-compensated waveform as input. FWHM of each compressed pulse  $\sim 48$  ps. (b) Blue: two bit period of the received signal. Red: simulated received signal generated by convolving target compensation waveform with the impulse response offline.

possible to retrieve the transmitted data through sampling and threshold detection.

Next we apply phase precompensation to the coded short pulses in experiments. The RF powers sent into the transmitter antenna, measured right after the receiver antenna and after the LNA are +10.08 dBm, -48.1 dBm and -19.80 dBm, respectively. Fig. 5(a) shows ten bit periods of the experimental measurement of the output signal at the receiver (coded as 1, 1, 1, -1, 1, -1, -1, 1, 1, 1). Compressed pulses ( $\sim 48$  ps FWHM) are present with both polarities. To evaluate the quality of the multipath compensation, we directly convolve the target pre-distorted waveform with the impulse response offline and plot the result in Fig. 5(b) in red. The close similarity between the experimental measurement (blue) and the simulation result indicates the channel sounding experiment is very accurate and our photonic RF-AWG generates waveforms with high fidelity. These observations serve as compelling evidence that to a very large extent, we have achieved the maximum pulse compression allowed by the channel and the phase-compensation algorithm. To assess the communication performance of our system, a pseudorandom sequence with length  $2^{17} - 1$  is transmitted as the data stream, and we re-sample the recorded waveform offline every 4 ns at the peak of each bit period. A threshold of 0 V is set to determine the transmitted information. No error is found over the full  $2^{17} - 1$  bit periods of the PN sequence, providing an upper bound to the bit error rate at the  $8 \times 10^{-6}$  level. Received signal-to-noise ratio (SNR), defined as the logarithm of the power ratio between the averaged peak voltage and the RMS voltage of the received signal without any input, is calculated to be  $\sim 22$  dB. The significant pulse compression is also confirmed by the open eye diagram shown in Fig. 6. We also plot the normalized positive peak voltage distribution together with a Gaussian fit in Fig. 7(b). In a noise-free setting, without any ISI, the received peak voltage is expected to have a constant

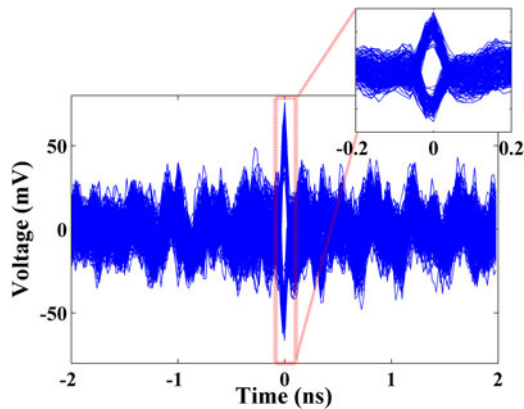


Fig. 6. Eye diagram of BPSK data modulated received signal, consisting 4000 overlapped bit periods. Inset: Horizontal magnification from  $-0.2$  to  $0.2$  ns.

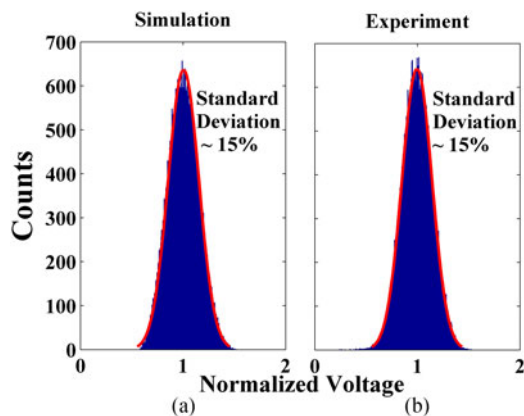


Fig. 7. Distributions of the received positive peak voltage, normalized to the average positive peak voltage. (a) Simulation, computed based on the target pre-compensation waveform, measured impulse response, and received SNR of 22 dB. Red: Gaussian fit. (b) Experimental result. Red: Gaussian fit.

value. When ISI is present and a particular peak is randomly affected by the sidelobes of its neighbor peaks, the peak voltage is assumed to have a random distribution. The concentration of the distribution, normally characterized by standard deviation (STD), directly indicates the level of ISI. In our experiment, the STD is found to be  $\sim 15\%$  at high SNR. This parameter matches very well with that of the simulation, which is calculated based on the target precompensation waveform, measured impulse response, and received SNR of 22 dB [as plotted in Fig. 7(a)]. The close resemblance between the simulation and experimental results and the fact that the average received positive peak voltage is  $\sim 6.7$  times the STD clearly demonstrates the substantial ISI suppression. According to the simulations of [12], the excellent performance of our system in mitigating ISI should allow scaling to several Gbits/s data rate if a higher repetition rate optical pulse source becomes available.

In another experiment, the transmitter antenna is moved to different positions in the vicinity of the spot marked in Fig. 1(b). Typically the distances between the placements are 20 cm or larger, while the separation between the transmitter and the receiver is maintained at approximately 6 meters. The channel impulse responses for 12 different transmitter positions are ob-

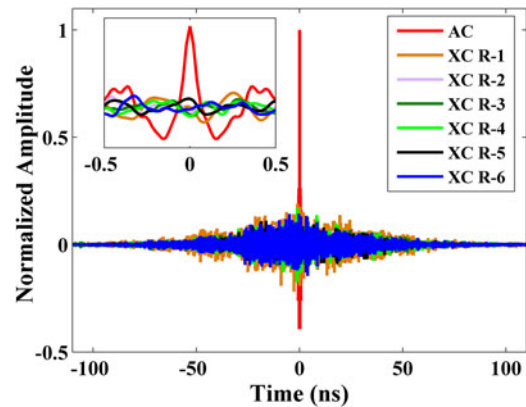


Fig. 8. Correlations of the measured impulse responses. Red: autocorrelation of the reference impulse response. Rest: cross-correlations between the reference and 6 other responses. Inset: zoom-in between  $-0.5$  and  $0.5$  ns.

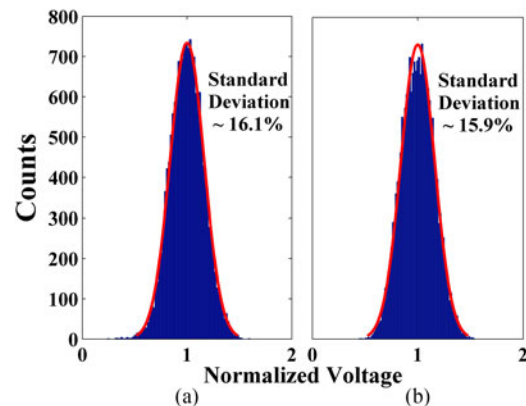


Fig. 9. Distributions of the received positive peak voltage, normalized to the average positive peak voltage. (a) From channel 4 (light green in Fig. 8). Received SNR 21.6 dB. Red curve: Gaussian fit. (b) From channel 6 (blue in Fig. 8). Received SNR 23.6 dB. Red curve: Gaussian fit.

tained using the sounding method described in Section III. As discussed in [14], UWB systems are characterized by short spatial coherent length (cm level). Consequently, even with a small antenna displacement, the impulse responses become uncorrelated. One impulse response is chosen as a reference whose autocorrelation is computed offline. The cross-correlations between the reference and all the other channel responses are also calculated. The average cross-correlation peak w.r.t. the reference auto-correlation peak is 14.3% with a STD of 2.9%. To illustrate, the autocorrelation of the reference (red curve), as well as six of the cross-correlations, are overlapped in Fig. 8. The inset to the figure clearly shows the low correlation between the channels. After repeating the spectral phase precompensation technique discussed in Section IV, error free (again bounded at  $8 \times 10^{-6}$ ) data transmission performance is achieved for all 12 channels. Experimental histograms analogous to that in Fig. 7 for two of these channels are plotted in Fig. 9; all the channels measured show similar results, with STDs ranging from 12.7% to 18.7%. These observations across multiple, nearly uncorrelated channels support the generality of the compensation results reported.

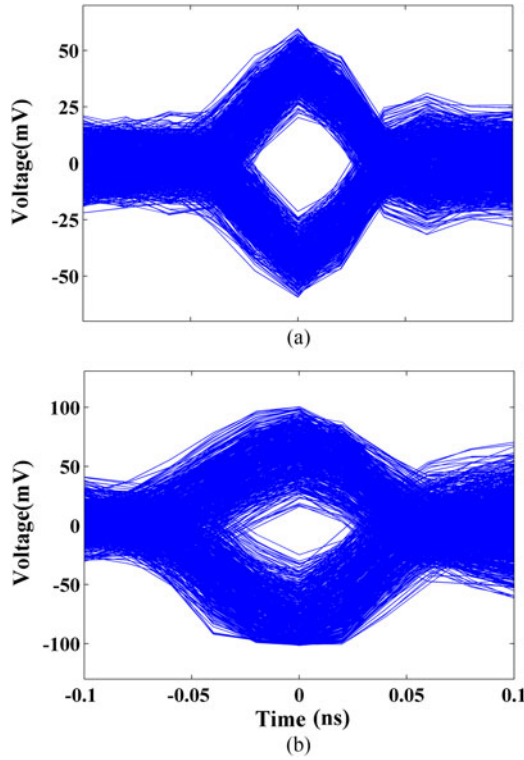


Fig. 10. Eye diagrams of received signals. (a) Phase compensated waveforms as input. (b) Time reversed waveforms as input.

## VI. PHASE COMPENSATION VERSUS TIME REVERSAL

To experimentally compare PC versus TR in dense multipath broadband indoor communication, we conduct a series of measurements. In the first experiment, predistorted waveforms are tailored based on the channel information shown in Fig. 3. Applying both phase-compensation and TR, compensation waveforms with the same time aperture (7.5 ns), same frequency coverage (2–18 GHz) and the same average optical input power to the photodetector ( $\sim 10$  dBm) are transmitted through the wireless channel. The received eye diagrams for PC and TR are plotted in Fig. 10(a) and (b), respectively. The averaged peak voltage for the PC case is  $\sim 42.8$  mV while that for the TR one is  $\sim 54$  mV. The increase in the averaged peak voltage magnitude (and thus the received SNR) of TR compared with PC arises because TR is equivalent to matched filtering, enabling highest achievable SNR at the center of the compressed peak for fixed transmit power [25]. However, the eye diagram observed with PC is clearly more open than that obtained with TR. As is well known, matched filtering is optimum for receivers limited by additive Gaussian noise [25]. However, PC is a better choice when limited by ISI. The difference in ISI suppression for PC and TR is also illustrated by the distributions of positive peak voltage (see Fig. 11). Despite the smaller mean voltage, the distribution of the PC case [see Fig. 11(a)] is more concentrated around the average value with a normalized STD of  $\sim 17\%$ . In contrast, although received at a higher voltage, the distribution of the TR case [see Fig. 11(b)] spreads significantly with a normalized STD of  $\sim 27\%$ , approximately 1.6 times larger than for PC. The STDs of the received positive peaks for PC and TR

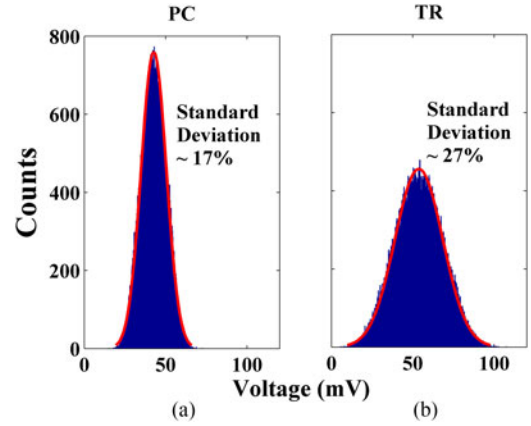


Fig. 11. Distributions of the received positive peak voltage. (a) Phase compensated waveforms as input. Red: Gaussian fit. (b) Time reversed waveforms as input. Red: Gaussian fit.

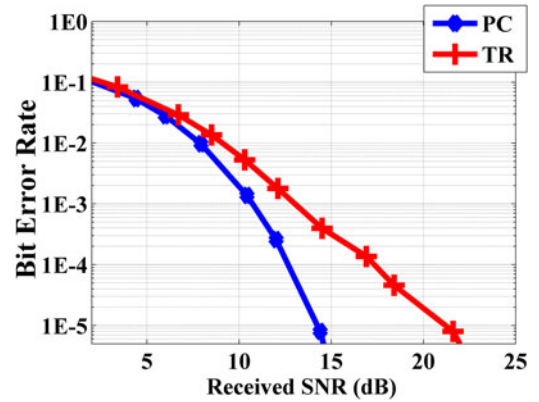


Fig. 12. Bit error rate against received signal to noise ratio. Blue: PC. Red: TR.

are also computed from the simulations based on the 12 actual channel measurements mentioned in Section V. The ratio of the STD of TR to that of PC ranges from 1.3 to 3.1, with an average value of 1.84. These observations provide evidence of the generality of our findings concerning the superiority of PC compared to TR in suppressing ISI over such UWB channels.

The BER performances of both compensation algorithms are also investigated. In this experiment, the precompensation waveforms (based on the channel shown in Fig. 3) are again synthesized with the same time aperture (7.5 ns) and the same frequency coverage (2–18 GHz) in both cases. Input powers are gradually adjusted to obtain the received SNR dependence of BERs, as presented in Fig. 12. In the low SNR regime, both BERs are dominated by the receiver noise. For PC, the BER reaches our sensitivity limit of  $8 \times 10^{-6}$  (set by the utilized PN sequence of length  $2^{17} - 1$ ) at  $\sim 15$  dB received SNR. For TR the BER curve decreases at a much slower rate, eventually reaching our error sensitivity limit at SNR  $\sim 23$  dB. Compared with the simulation in [12], the BER curve of TR does not level off at high SNR, primarily because of the smaller delay spread ( $\sim 17.1$  ns) of the impulse response here. Nevertheless, our experimental results clearly confirm the enhanced BER performance of PC compared with TR.

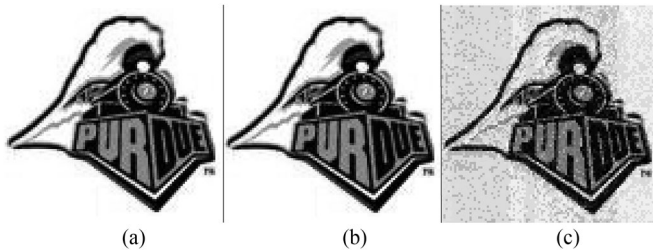


Fig. 13. Experimental demonstration of image transmission. (a) Original image. (b) Reconstructed image when PC is used, measured SNR  $\sim 15$  dB. (c) Reconstructed image when TR is used, measured SNR  $\sim 17.2$  dB.

To visually illustrate the advantage of PC over TR, a grayscale image of a logo of Purdue University [see Fig. 13(a)] is transmitted over the channel (see Fig. 3). The  $100 \times 100$  pixels are transmitted in column by column format, with each pixel encoded by 8 bits. The optical powers sent into the photodetector for PC and TR are kept the same. Fig. 13(b) is the reconstructed image at the receiver when PC is utilized, with a measured SNR of 15 dB. The picture is free of any visually observable error. In contrast, when TR is used, the reconstructed image [see Fig. 13(c)] is obviously contaminated, even with higher measured SNR (17.2 dB). This experiment again substantiates the improved ISI suppression performance of PC compared to TR in broadband indoor communications with strong multipath.

## VII. DISCUSSION AND CONCLUSION

In this paper we discuss a photonic ultra-broadband RF wireless communication system spanning 2–18 GHz and demonstrate error-free data transmission in BPSK format over dense-multipath channels. For the first time to our knowledge, we report a direct experimental comparison between TR and PC in data transmission over a strong multipath channel. Our results confirm predictions that PC significantly enhances suppression of intersymbol interference. These experiments suggest that photonic methods may play a role not only in transport of wireless signals but also for signal processing related to indoor multipath wireless communications.

Our system could be further improved in several aspects. For instance, by replacing the dual pulse shaper scheme used here with the single pulse shaper, interferometric RF-AWG configuration reported in [26], system complexity will be reduced. Furthermore, this configuration has been demonstrated to support higher order modulation formats with potential for multiple bits per symbol. Our current experiment covers the frequency range from 2 to 18 GHz, with the purpose of emphasizing the large bandwidth capability of photonic RF-AWG. However, most of the energy arriving at the receiver is below  $\sim 10$  GHz due to the higher attenuation at higher frequencies [refer to the frequency response shown in Fig. 3(b)]. Better spectral efficiency with little communication performance degradation should be achievable when the RF frequency is confined below 10 GHz.

The data rate and spectral efficiency in the current experiments are limited by the 250 MHz repetition rate of the mode-locked laser source. It should be possible to improve both by utilizing a higher repetition rate optical source. Modest repetition rate enhancement (up to few GHz) can be accomplished using

compact mode-locked lasers [27], [28], or by employing an optical pulse interleaver [29]. Moving beyond a few GHz, one can utilize optoelectronic combs [30], [31], which provide additional flexibility in choice of center frequency, bandwidth, and repetition rate. In addition, the RF oscillator used to drive the optoelectronic comb can dually serve as a clock in order to synchronize with other electronics without the need for optoelectronic conversion of the pulse train. Stepping further in the future, one can look to photonic integration technology as a path to reduce the scheme footprint while also enhancing scalability options outside of the laboratory. Recent progress on optical frequency comb generation via nonlinear wave mixing in microring resonators has resulted broadband optical signals with repetition rates in the low tens of GHz range, e.g., [32], [33]. While these repetition-rates still remain on the high-end for this current application, the field has witnessed continual advancement towards lower repetition rates.

In addition to integrated micro-comb technology, there has been recent research directed towards photonically integrated optical pulse shapers [34]–[40]. Besides providing a further reduction in device footprint, some integrated pulse shaping demonstrations like [34], [38], [40], utilize active modulation elements, (i.e. SOAs, EAMs), which provide reconfiguration speeds that are orders of magnitude faster than traditional bulk liquid crystal devices (typically limited to millisecond update rates). Increasing the shaper update rate would allow the system to more readily compensate the channel-antenna link for application in dynamic environments. Indeed, the aforementioned pulse shaping demonstrations combined with the booming progress in large-scale photonic integration technology - motivated by lightwave telecom applications [41] - provide a host of new possibilities for integrating RF-photonic applications like ours.

Last but not least, although photonic approaches are utilized here, we can also exploit the fast update speed of electronic waveform generation approach. The principles demonstrated here using photonic technologies could provide guidance to future implementations based on broadband electronics.

## ACKNOWLEDGMENT

The authors would like to thank Dr. A. J. Metcalf for his contribution to the Discussion and Conclusion section.

## REFERENCES

- [1] D. Porcino and W. Hirt, "Ultra-wideband radio technology: Potential and challenges ahead," *IEEE Commun. Mag.*, vol. 41, no. 7, pp. 66–74, Jul. 2003.
- [2] G. R. Aiello and G. D. Rogerson, "Ultra-wideband wireless systems," *IEEE Microw. Mag.*, vol. 4, no. 2, pp. 36–47, Jun. 2003.
- [3] L. Yang and G. B. Giannakis, "Ultra-wideband communications: An idea whose time has come," *IEEE Signal Process. Mag.*, vol. 21, no. 6, pp. 26–54, Nov. 2004.
- [4] M. G. Di Benedetto, *UWB Communication Systems: A Comprehensive Overview*, vol. 5. New York, NY, USA: Hindawi, 2006.
- [5] J. D. Taylor, *Introduction to Ultra-Wideband Radar Systems*. New York, NY, USA: Taylor & Francis, 1994.
- [6] R. C. Qiu, H. P. Liu, and X. M. Shen, "Ultra-wideband for multiple access communications," *IEEE Commun. Mag.*, vol. 43, no. 2, pp. 80–87, Feb. 2005.
- [7] H. Shams, A. Kaszubowska-Anandarajah, P. Perry, and L. P. Barry, "Optical generation, fiber distribution and air transmission for ultra wide band

- over fiber system," in *Proc. Conf. Opt. Fiber Commun.*, 2009, vol. 1–5, pp. 2814–2816.
- [8] R. R. Lopez, A. Caballero, X. B. Yu, T. B. Gibbon, J. B. Jensen, and I. T. Monroy, "A comparison of electrical and photonic pulse generation for IR-UWB on fiber links," *IEEE Photon. Technol. Lett.*, vol. 22, no. 5, pp. 263–265, Mar. 2010.
- [9] S. L. Pan and J. P. Yao, "UWB-over-fiber communications: Modulation and transmission," *J. Lightw. Technol.*, vol. 28, no. 16, pp. 2445–2455, Aug. 2010.
- [10] X. B. Yu, T. B. Gibbon, R. Rodes, T. T. Pham, and I. T. Monroy, "System wide implementation of photonically generated impulse radio ultra-wideband for gigabit fiber-wireless access," *J. Lightw. Technol.*, vol. 31, no. 2, pp. 264–275, Jan. 2013.
- [11] I. H. Naqvi *et al.*, "Experimental validation of time reversal ultra wide-band communication system for high data rates," *IET Microw. Antennas Propag.*, vol. 4, pp. 643–650, May 2010.
- [12] A. Dezfouliyan and A. M. Weiner, "Phase compensation communication technique against time reversal for ultra-wideband channels," *IET Commun.*, vol. 7, pp. 1287–1295, Aug. 2013.
- [13] Y. Li and A. M. Weiner, "Photonic-assisted broadband wireless communication with on-line channel compression," in *Opt. Comm. Conf.*, 2015, paper W3F.3.
- [14] A. Dezfouliyan and A. M. Weiner, "Microwave photonics for space-time compression of ultrabroadband signals through multipath wireless channels," *Opt. Lett.*, vol. 38, pp. 4946–4949, Dec. 2013.
- [15] A. M. Weiner, "Ultrafast optical pulse shaping: A tutorial review," *Opt. Commun.*, vol. 284, pp. 3669–3692, Jul. 2011.
- [16] J. Chou, Y. Han, and B. Jalali, "Adaptive RF-photonic arbitrary waveform generator," *IEICE Trans. Electron.*, vol. E86c, pp. 1226–1229, Jul. 2003.
- [17] I. S. Lin, J. D. McKinney, and A. M. Weiner, "Photonic synthesis of broadband microwave arbitrary waveforms applicable to ultra-wideband communication," *IEEE Microw. Wireless Compon. Lett.*, vol. 15, no. 4, pp. 226–228, Apr. 2005.
- [18] A. Dezfouliyan and A. M. Weiner, "Photonic synthesis of high fidelity microwave arbitrary waveforms using near field frequency to time mapping," *Opt. Exp.*, vol. 21, pp. 22974–22987, Sep. 2013.
- [19] Y. Li, A. Rashidinejad, J.-M. Wun, D. E. Leaird, J.-W. Shi, and A. M. Weiner, "Photonic generation of W-band arbitrary waveforms with high time-bandwidth products enabling 3.9 mm range resolution," *Optica*, vol. 1, pp. 446–454, Dec. 2014.
- [20] Y. Li, A. Dezfouliyan, and A. M. Weiner, "Photonic synthesis of spread spectrum radio frequency waveforms with arbitrarily long time apertures," *J. Lightw. Technol.*, vol. 32, no. 20, pp. 3580–3587, Oct. 2014.
- [21] A. Dezfouliyan and A. M. Weiner, "Evaluation of time domain propagation measurements of UWB systems using spread spectrum channel soundings," *IEEE Trans. Antennas Propag.*, vol. 60, no. 10, pp. 4855–4865, Oct. 2012.
- [22] A. Dezfouliyan and A. M. Weiner, "Experimental investigation of UWB impulse response and time reversal technique up to 12 GHz: Omnidirectional and directional antennas," *IEEE Trans. Antennas Propag.*, vol. 60, no. 7, pp. 3407–3415, Jul. 2012.
- [23] R. C. Qiu, Z. Chenming, Z. John Qiang, and G. Nan, "Channel reciprocity and time-reversed propagation for ultra-wideband communications," in *Proc. IEEE Antennas Propag. Soc. Int. Symp.*, 2007, pp. 29–32.
- [24] M. Fink, "Time-reversal of ultrasonic fields .1. Basic principles," *IEEE Trans. Ultrason., Ferroelect., Freq. Control*, vol. 39, no. 5, pp. 555–566, Sep. 1992.
- [25] M. B. Pursley, *Introduction to Digital Communications*. Upper Saddle River, NJ, USA: Prentice Hall, 2005.
- [26] A. Rashidinejad, D. E. Leaird, and A. M. Weiner, "Ultrabroadband radio-frequency arbitrary waveform generation with high-speed phase and amplitude modulation capability," *Opt. Exp.*, vol. 23, pp. 12265–12273, May 2015.
- [27] H. Byun *et al.*, "Compact, stable 1 GHz femtosecond Er-doped fiber lasers," *Appl. Opt.*, vol. 49, pp. 5577–5582, Oct. 2010.
- [28] H.-W. Chen, G. Chang, S. Xu, Z. Yang, and F. X. Kärtner, "3GHz, fundamentally mode-locked, femtosecond Yb-fiber laser," *Opt. Lett.*, vol. 37, pp. 3522–3524, Sep. 2012.
- [29] A. Haboucha *et al.*, "Optical-fiber pulse rate multiplier for ultralow phase-noise signal generation," *Opt. Lett.*, vol. 36, pp. 3654–3656, Sep. 2011.
- [30] A. J. Metcalf, V. Torres-Company, D. E. Leaird, and A. M. Weiner, "High-power broadly tunable electrooptic frequency comb generator," *IEEE J. Sel. Topics Quantum Electron.*, vol. 19, no. 6, pp. 231–236, Nov./Dec. 2013.
- [31] V. Torres-Company and A. M. Weiner, "Optical frequency comb technology for ultra-broadband radio-frequency photonics," *Laser Photon. Rev.*, vol. 8, pp. 368–393, 2014.
- [32] A. R. Johnson *et al.*, "Chip-based frequency combs with sub-100 GHz repetition rates," *Opt. Lett.*, vol. 37, pp. 875–877, Mar. 2012.
- [33] J. Pfeifle *et al.*, "Coherent terabit communications with microresonator Kerr frequency combs," *Nature Photon.*, vol. 8, pp. 375–380, Feb. 2014.
- [34] M. J. R. Heck *et al.*, "Design, fabrication and characterization of an InP-based tunable integrated optical pulse shaper," *IEEE J. Quantum Electron.*, vol. 44, no. 4, pp. 370–377, Apr. 2008.
- [35] N. K. Fontaine *et al.*, "Compact 10 GHz loopback arrayed-waveguide grating for high-fidelity optical arbitrary waveform generation," *Opt. Lett.*, vol. 33, pp. 1714–1716, Aug. 2008.
- [36] R. P. Scott, N. K. Fontaine, J. P. Heritage, and S. J. B. Yoo, "Dynamic optical arbitrary waveform generation and measurement," *Opt. Exp.*, vol. 18, pp. 18655–18670, Aug. 2010.
- [37] M. H. Khan *et al.*, "Ultrabroad-bandwidth arbitrary radiofrequency waveform generation with a silicon photonic chip-based spectral shaper," *Nature Photon.*, vol. 4, pp. 117–U30, Feb. 2010.
- [38] S. Tahvili *et al.*, "InP-based integrated optical pulse shaper: Demonstration of chirp compensation," *IEEE Photon. Technol. Lett.*, vol. 25, no. 5, pp. 450–453, Mar. 2013.
- [39] J. Wang *et al.*, "Reconfigurable radio-frequency arbitrary waveforms synthesized in a silicon photonic chip," *Nature Commun.*, vol. 6, Jan. 2015, Art. no. 5957.
- [40] A. J. Metcalf *et al.*, "Integrated optical pulse shaping: SOA amplitude control and sub-microsecond switching of 32 channels at 25 GHz spacing," in *Proc. CLEO*, San Jose, CA, USA, 2016, Art. no. SM4L.6.
- [41] R. Nagarajan *et al.*, "InP photonic integrated circuits," *IEEE J. Sel. Topics Quantum Electron.*, vol. 16, no. 5, pp. 1113–1125, Sep./Oct. 2010.

**Yihan Li** was born in Xuzhou, China, in 1988. He received the B.S. degree in optical information science and technology from the University of Science and Technology of China (USTC), Hefei, China, in 2010, and the Ph.D. degree in electrical engineering from Purdue University, West Lafayette, IN, USA, in 2015.

From 2008 to 2010, he was a Research Assistant with the Key Laboratory of Optoelectronic Science and Technology, USTC. In 2010, he was a Research Assistant with the Institute of Physics, Chinese Academy of Science, Beijing, China. From 2010 to 2015, he was a Research Assistant with the Ultrafast Optics and Optical Fiber Communications Laboratory, Purdue University. He joined IMRA America, Boulder Research Lab as a Laser Research Scientist in 2015. His research interests include ultrafast optics, optical pulse shaping, microwave photonics, and broadband RF wireless communications.

**Andrew M. Weiner** received the Sc.D. degree in electrical engineering from Massachusetts Institute of Technology, Cambridge, MA, USA, in 1984.

He joined Bellcore, at that time a premier telecommunications industry research organization, first as a Member of Technical Staff and later as a Manager of Ultrafast Optics and Optical Signal Processing Research. He is the Scifres Family Distinguished Professor of electrical and computer engineering. In 2008, he was elected to membership in the National Academy of Engineering and in 2009 was named a Department of Defense National Security Science and Engineering Faculty Fellow. He recently served a three year term as a Chair of the National Academy's U.S. Frontiers of Engineering Meeting; at present he serves as an Editor-in-Chief of *Optics Express*, an all-electronic, open access journal publishing more than 3000 papers a year emphasizing innovations in all aspects of optics and photonics. He joined Purdue as a Professor in 1992, and has since graduated more than 30 Ph.D. students. He has also spent sabbaticals at the Max Born Institute for Nonlinear Optics and Ultrashort Pulse Spectroscopy, Berlin, Germany and at JILA, University of Colorado and National Institute of Standards and Technology, Boulder, Colorado. He is especially well known for his pioneering work on programmable generation of arbitrary ultrashort pulse waveforms, which has found application both in fiber optic networks and in ultrafast optical science laboratories around the world. He is the author of a textbook entitled *Ultrafast Optics*, has published 8 book chapters, more than 300 journal articles, more than 500 conference papers, and is the inventor of 16 U.S. patents. His research interests include ultrafast optics, with a focus on processing of extremely high speed lightwave signals and ultrabroadband radio-frequency signals.

Prof. Wiener received the Hertz Foundation Doctoral Thesis Prize (1984), the Optical Society of America's Adolph Lomb Medal (1990) and R.W. Wood Prize (2008), the International Commission on Optics Prize (1997), and the IEEE Photonics Society's William Streifer Scientific Achievement Award (1999) and Quantum Electronics Prize (2011). At Purdue he has been recognized with the inaugural Research Excellence Award from the Schools of Engineering (2003), the Provost's Outstanding Graduate Student Mentor Award (2008), the Herbert Newby McCoy Award for outstanding contributions to the natural sciences (2013), and the College of Engineering Mentoring Award (2014).